MRS Communications (2017), *7*, 832–839

doi:10.1557/mrc.2017.113

MRS Communications

Research Letter

Dynamics of interacting interphases in polymer bilayer thin films

David D. Hsu, Department of Physics & Engineering, Wheaton College, 501 College Avenue, Wheaton, IL 60187, USA
Wenjie Xia, Materials Science and Engineering Division, National Institute of Standards and Technology, 100 Bureau Drive, M/S 8550, Gaithersburg, MD 20899, USA; Center for Hierarchical Materials Design, Northwestern University, Evanston, IL 60208, USA; Department of Civil & Environmental Engineering, Northwestern University, 2145 Sheridan Road, Evanston, IL 60208, USA
Jake Song, Department of Materials Science & Engineering, Massachusetts Institute of Technology, 77 Massachusetts Avenue, Cambridge, MA 02139, USA; Department of Materials Science & Engineering, Northwestern University, 2145 Sheridan Road, Evanston, IL 60208, USA
Sinan Keten, Department of Civil & Environmental Engineering, Northwestern University, 2145 Sheridan Road, Evanston, IL 60208, USA; Department of Mechanical Engineering, Northwestern University, 2145 Sheridan Road, Evanston, IL 60208-3109, USA

Address all correspondence to Sinan Keten at **s-keten@northwestern.edu**

(Received 14 July 2017; accepted 28 September 2017)

Abstract

We investigate how the local glass-transition temperature (T_g) depends on film thickness in monolayer and bilayer thin films with a polystyrene (PS) upper-layer and a poly(methyl methacrylate) (PMMA) lower-layer using coarse-grained simulations. Interactions between overlapping interphases demonstrate a superposition principle for describing their glass-transition behaviors. For supported bilayer films, the free surface effect on a PS film upper-layer is effectively eliminated due to an enhanced local T_g near the PS–PMMA interface, which cancels out depressed T_g near the free surface. However, at very low PMMA lower-layer thicknesses, the PMMA-substrate effect can penetrate through the polymer–polymer interface, leading to enhanced T_g in the PS upper-layer.

Introduction

In nanoscale films, regions near interfaces exhibit properties which are strongly perturbed from their respective bulk identities, such as modulus, glass-transition temperature (T_g), density and relaxation dynamics, known as the nanoconfinement effect. As the characteristic size of the material decreases, these "interphase" regions constitute a larger fraction of the material by volume, and can greatly influence the macroscopic properties.[1–4] Significant efforts have been carried out to quantify the extent to which polymer–air[1,3–6] and polymer–substrate[7–9] interfaces cause deviation from bulk properties for nanoscopically thin films. However, the behavior of polymer–polymer "soft" interfaces[10–16] occurring at the junction of immiscible polymers is far less understood. Interphases formed near these discontinuities approach each other as the characteristic feature dimensions become small. Our understanding of the interactions of these interphases, specifically whether they have additive or subtractive effects in thin films remains to be clarified.

Previous studies have shown that the nanoconfinement behavior of a polymer thin film can be highly sensitive to the presence of an underlying polymer layer, with mobility becoming altered by several orders of magnitude depending on the chemical species. A study was performed by Roth et al.[10] on multilayer films of PMMA and PS using fluorescence microscopy, in which a fluorescent dye molecule was chemically bonded to polymer chains to allow for local estimation of the T_g. It was observed that the outermost 14 nm layer of a supported PS film underwent a ~32 K T_g reduction due to the free surface effect. However, this effect could be effectively eliminated when the PS film was placed atop a PMMA or P2VP supported layer of arbitrary thickness. Yoon and McKenna carried out a similar experiment using a direct dynamic particle embedment method and found that the T_g in the upper layer probed by the particle underwent a less than 10 K reduction compared with the bulk, regardless of the lower-layer material.[11] More recently, Baglay and Roth used fluorescence microscopy to determine the local T_g profile in polystyrene-poly(n-butyl methacrylate) (PS-PnBMA) bilayer films near the polymer–polymer interface.[14] They observed that despite only a 7 nm interface thickness in the physical composition profile, the distance over which the local T_g was perturbed from the bulk persists 350 nm into the rubbery PnBMA (293 K bulk T_g) layer and nearly 400 nm into the glassier PS (373 K bulk T_g) layer.

Despite a large body of experimental and simulation work which focused on mobility and free volume disturbances at various interfaces,[1,17] there is still considerable effort to be undertaken to characterize the local gradients in T_g at sub-10 nm resolution near polymer–air, polymer–substrate, and polymer–polymer interfaces. Existing experimental methods have difficulty probing the local T_g for layers at nanometer scale resolution, and the generic nature of simulations may not adequately represent the true thermomechanical behavior of a specific polymer material. Furthermore, there has been

minimal work done to predict the combined T_g-nanoconfinement effect at the coalescence of various interphase types, which is pertinent in understanding the physical behavior of ultrathin films.

In the present study, we utilize polymer-specific coarse-grained (CG) models informed from atomistic systems to predict the local and system-averaged effects on T_g due to the various interface types in PS and PMMA homopolymer films and bilayers. A PMMA lower-layer and a PS upper-layer are then combined within a supported bilayer system to understand how the various interphases interact below critical length scales (illustrated in Fig. 1). We then aim to establish a framework for predicting the effective local T_g gradient for regions that are perturbed from the bulk properties as the result of more than one interphase type for ultrathin films.

Simulation methodology

We utilize polymer-specific CG models for PS and PMMA, which have been developed by our Thermomechanically Consistent Coarse-Graining (TCCG) method.[18,19] In these CG models, the bulk T_g (371 and 396 K for PS and PMMA, respectively) has been tuned to that of the all-atomistic models by varying cohesive interactions. (See Tables SI–SIII for CG force field parameters in the Supporting Information.) PS freestanding thin films of varying thickness from 10 to 60 nm are generated using a random walk algorithm. We use 200 repeat units per chain and vary the number of chains to achieve the desired thickness, while maintaining a 9×9 nm^2 cross section that is periodic in the x and y-directions. The z dimension (thickness direction) is non-periodic, and adequate space in the simulation box is allotted above the film surface to simulate the polymer–air interface. This also allows the system to expand and contract freely in the z-direction and is therefore effectively equivalent to an NPT ensemble with zero pressure at the film surfaces.

To model the substrate for supported PS and PMMA films, we add an implicit attractive wall, which interacts with the film through a Lennard–Jones 12–6 potential with resulting energy function of the form:

$$E_{sp} = 4\varepsilon_{sp}\left[\left(\frac{\sigma}{r}\right)^{12} - \left(\frac{\sigma}{r}\right)^{6}\right], \quad r < r_c, \tag{1}$$

where ε_{sp} is the substrate–polymer interaction energy equal to 10 kcal/mol to ensure that a clear interphase and strong enhancement of the local T_g is achieved near the substrate interface. σ is defined as the point at which the energy crosses the zero line and is 4.5 Å to be consistent with the CG bead non-bonded parameter. The cutoff distance r_c is set to 15 Å, similar to that of the non-bonded cohesive interactions.

For supported PS-PMMA bilayer films, we generate films with 12×12 nm^2 cross sections in the x-y plane for improved sampling during local T_g estimation. A PMMA lower-layer with a variable thickness from 2 to 36 nm in the z-direction and a PS upper-layer of 18 nm are generated. We enforce a reflective wall between the under- and over-layers to prevent beads from intermixing during the soft potential push-off step. Subsequently, we remove the reflective wall and employ an implicit attractive Lennard–Jones wall at the bottom surface of the PMMA lower-layer. We note that the attractive wall does not interact with the upper PS layer due to the short cutoff distance.

After these systems are generated, in the initial annealing step, we first minimize the system using the conjugate gradient method,[20] perform a soft potential push-off step, and then cycle the temperature between 210 and 750 K over a period of 4 ns using the Nose-Hoover[21] NPT ensemble until the energy and density have converged. For all simulations, we use a 4 fs timestep and carry out calculations with the LAMMPS molecular dynamics software.[22]

The T_g of the overall film is estimated by calculating the α-relaxation time τ_α via the self-part of the intermediate scattering function $F_s(q, t)$ as described in our previous work.[5] The α-relaxation time τ_α is taken to be when $F_s(q, t)$ decays to 0.2. We use a computational measure of T_g, which is estimated as the temperature at which τ_α reaches 1 ns.[5,23] To capture the local T_g, the film is divided into 2 nm layers along the z-axis, and the local $F_s(q, t)$ is employed to determine the local τ_α of each layer. The T_g of each bin layer is calculated for at least 5 samples, and the data sets presented in this work are based on the average T_g values for each bin.

Results and discussion

Monolayer thin film systems

To understand how nanoconfinement behavior due to the free surface interface is affected by the film thickness, the local T_g is calculated for freestanding monolayer PS thin films of various thicknesses. To isolate the free surface interphase T_g profile, we use films that are sufficiently thick to ensure that the interphase regions at each of the two surfaces do not overlap. For PS freestanding films, we use a ~40 nm film thickness for which the local T_g converges to a constant value in the interior region [Fig. 2(a)]. The PS film local T_g profile experiences about 28 K depression relative to the bulk at the outermost 2 nm surface region. It converges to a constant value at 12 nm, and remains relatively constant within the ~16 nm interior region.

The local T_g profile at the free surface interphase region can be described by the exponential function:

$$\Delta T_g^{fs}(z) = -A^{fs} e^{(-z/\lambda^{fs})}, \tag{2}$$

where ΔT_g^{fs} is defined as the bulk-like interior T_g substracted from the local freestanding film T_g. A^{fs} and λ^{fs} are empirical fitting parameters relating to the strength of the free surface effect and the characteristic length of the interphase, respectively. This is supported by other computational studies reporting the local T_g at the free surface, which could also be well described by the exponential function.[4,24] A^{fs} and λ^{fs} for our PS model are found to be 22.7 K and 2.5 nm, respectively.

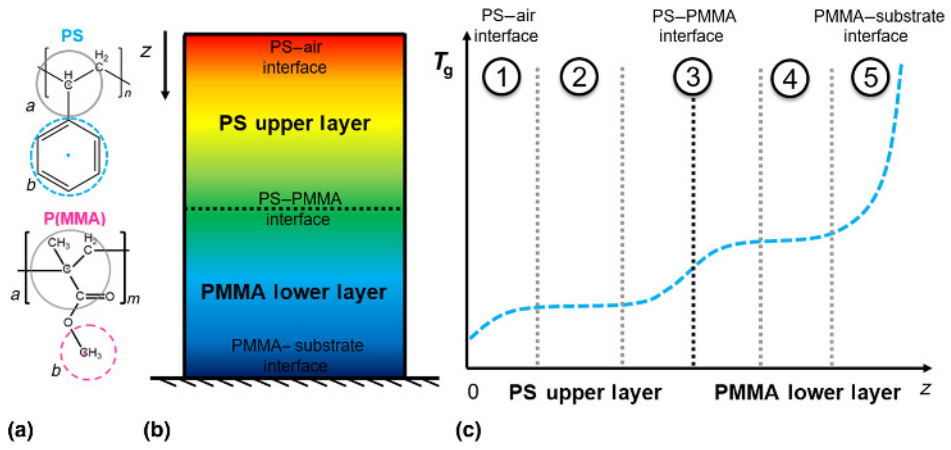

Figure 1. (a) Coarse-grained mapping scheme for PS and PMMA models. (b) Bilayer system schematic consisting of a PMMA lower-layer and PS upper-layer depicting local T_g gradient. (c) Schematic representation of the local T_g versus z position and distinct T_g transition regions.

The fitting results are shown as dashed lines in Fig. 2(a) and a summary of all fitting parameters are shown in Table SIV. Beyond interphase regions, the local τ_α converges to a constant value, indicating a bulk-like interior of the film.[5] We find that the interphase region size is nearly independent of the overall film thickness. This implies that there is a critical thickness H_{crit}^{fs} for the polymer film, below which the two interphase regions (i.e., film top and bottom free-surface layers) may begin to interact.[25] In the case of the freestanding thin films, H_{crit}^{fs} can simply be taken to be approximately twice the free surface interphase length scale $2\xi^{fs}$, which is ~24 nm for the PS model. We find that the free surface gradient profile appears to be independent of the film thickness for PS films above H_{crit}^{fs}. This result supports the findings from Tito et al. which also demonstrated that the interphase region behavior is not affected by film thickness as long as interphases do not overlap.[12]

Interestingly, the PS film interior does not appear to reach the bulk T_g even for film thicknesses well over 40 nm. Although the PS film converges to a constant T_g of 362 K in the center of the film, this is ~7 K below the T_g found for bulk PS simulations. This is similar to the results recently reported by Rissanou and Harmandaris,[26] where they find that the local segmental relaxation time for all-atomistic models of PS films supported by multi-layer graphene does not converge precisely to the bulk in the interior region for 12 nm films. However, Zhou and Milner do find the convergence of the T_g within the film interior when using a united atom model for freestanding PS films.[24] This discrepancy deserves additional investigation in future work. However, we do not expect this to affect the results reported in this study as we compare local T_g perturbations to the "bulk-like" interior T_g in ΔT_g calculations and local T_g gradient functions.

We next examine the local T_g for films thinner than H_{crit}^{fs} to investigate the physical behavior of films where the interphase regions presumably intersect. For these systems, no interior convergence region is found, but rather a cusp at the local T_g maximum and greater T_g depression at the outermost free surfaces is observed in Fig. 2(a). We find that the superposition of analytical functions that we employed to describe the local T_g can capture film behavior down to 10 nm thick films as a reasonable approximation. This finding indicates that when the film is sufficiently thin that free surface interphases begin to interact, their combined effects can be well approximated to be additive. Therefore, we can describe the local T_g of freestanding thin films by the following expression:

$$\Delta T_g^{fs}(z) = -A_i^{fs}\left(e^{(-z/\lambda_i^{fs})} + e^{((z-H)/\lambda_i^{fs})}\right), \quad (3)$$

where the first and second exponential terms in the expression represent the lower and upper free surfaces, respectively. We find that this expression holds for all film thicknesses tested, both above and below H_{crit}^{fs} down to ~10 nm.

Now that we have established the influence of free surfaces, we now apply a similar analysis to supported PMMA thin films. Supported films demonstrate an interphase region of reduced local T_g near the free surface with length scale ξ^{fs}, as well as an interphase region of enhanced local T_g near the attractive substrate with length scale ξ^{sp}.[7,8,17] Therefore, we begin by assuming that a critical thickness exists for supported films above which free surface and supported interphases do not interact. This can be expressed as $H_{crit}^{sp} = \xi^{fs} + \xi^{sp}$. We find ξ^{sp} for both PS and PMMA by capturing the length scale near the supporting substrate, where the local T_g profile for 40 nm PS and PMMA supported films converges to the bulk. We simulate supported films for PS and PMMA with thicknesses varying from 10 to 40 nm. In this case, both PS and PMMA films are supported by an implicit wall with an interaction energy $\varepsilon_{sp} = 10$ kcal/mol. Although commonly used substrate materials such as silica will adhere with different strengths to PS and PMMA films (i.e., greater adhesion energy

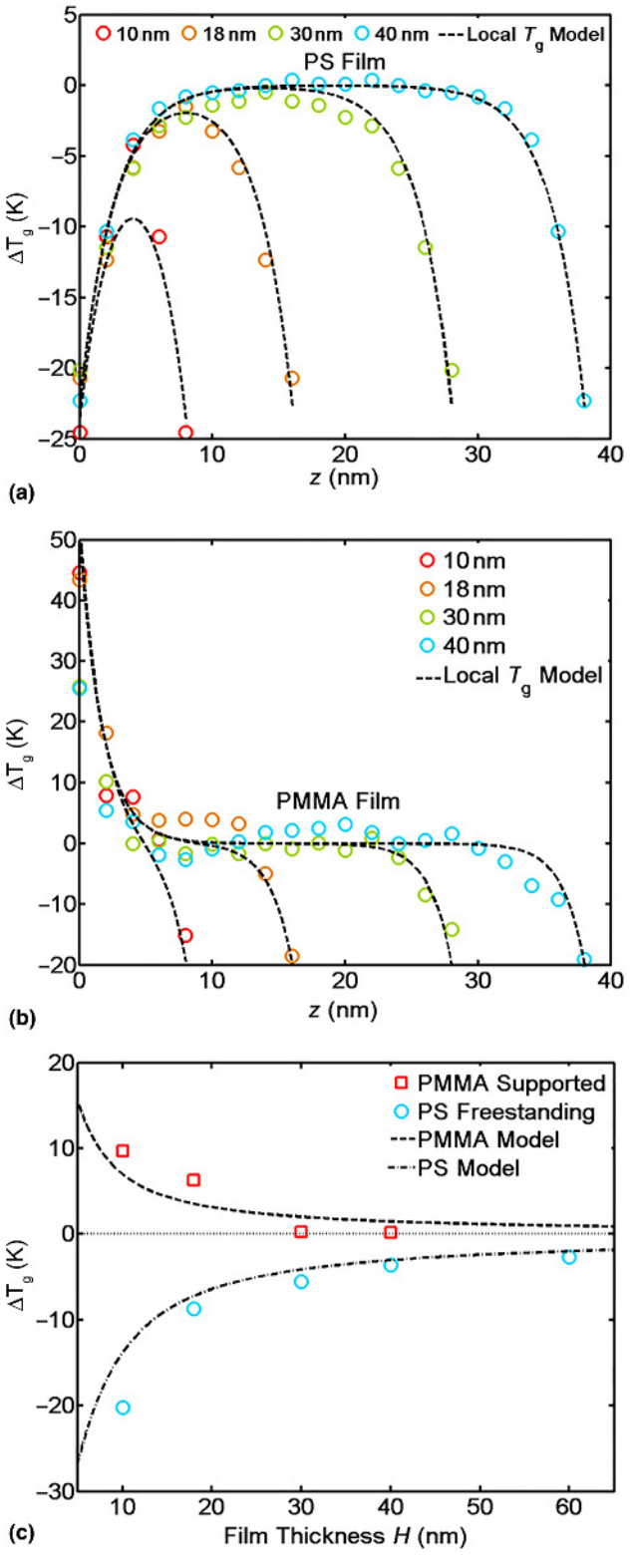

Figure 2. (a) Comparison of simulated local ΔT_g depression in PS freestanding films and superposition model. (b) Local ΔT_g profile for PMMA supported films compared with superposition model. (c) Overall T_g of freestanding PS and supported PMMA versus film thickness from simulations and superposition model.

for PMMA due to the hydrogen-bonding with silica substrate), we choose to use a similar adhesion energy in order to directly compare substrate effects on these two systems resulting from differences in polymer chemistry.

For sufficiently thick films, we see an isolated region of T_g depression near the free surface with behavior that matches our observations for the freestanding condition for both polymers. [See Fig. 2(b) for PMMA supported results and Fig. S2 for PS.] We find that the same analytical local T_g parameters in Eq. (3) for the freestanding condition can readily capture the behavior in the free surface region of supported films thicker than a critical size. In the 2 nm region nearest to the substrate, we see a region in which T_g is enhanced. For PMMA, T_g appreciates 40 K above the bulk value and converges to a constant value ~8 nm from the substrate. For PS, T_g enhancement is up to 50 K greater than the bulk and converges to the interior region at ~9 nm. Note that these large T_g enhancements are due to a large interaction energy, which is used to highlight the substrate effect. The differences in magnitudes of the T_g enhancement for PS and PMMA may be a result of chemical structure details, particularly pertaining to the bulkiness of backbone versus sidechain groups. In another study, we found that the degree of T_g enhancement at an attractive substrate relative to the bulk can change with varying side-group size.[27] Comparisons between the effects of chemical structure on substrate T_g nanoconfinement effect in PS and PMMA supported films is reserved for a future study.

Based on these measurements, the critical thickness H_{crit}^{sp} of PS is found to be ~21 nm ($\xi_{PS}^{fs} = 12$ nm, $\xi_{PS}^{sp} = 9$ nm) and ~15 nm ($\xi_{PMMA}^{fs} = 7$ nm, $\xi_{PMMA}^{sp} = 8$ nm) for PMMA. Measuring the local T_g profile for films below the critical thickness, we find that within regions where the interphases overlap, the behavior follows the superposition of supported and free surface interphase regions. This suggests that the interaction between gradient profiles of dissimilar interphase types can be approximated as additive as well. Therefore, the entire supported film profile can be described by superposed exponential functions to describe the substrate and free surface interphase regions:

$$\Delta T_{g,i}^{sp}(z) = A_i^{sp} e^{(-z/\lambda_i^{sp})} - A_i^{fs} e^{((z-H)/\lambda_i^{fs})} \quad (4)$$

with parameters developed for PS and PMMA with $\varepsilon_{sp} = 10$ kcal/mol shown in Table SIV of the Supporting Information. Again, A^{sp} and λ^{sp} are related to the strength of T_g enhancement and the length scale over which T_g enhancement persists. Values for PS are found to be 60.5 K and 2.1 nm for A^{sp} and λ^{sp}, respectively, and 52.0 K and 1.7 nm for PMMA. This reflects a slightly greater T_g enhancement effect on PS than for PMMA for equal substrate attraction energy as discussed earlier. The results for the PMMA local T_g model are shown in Fig. 2(b), and PS results are shown in Fig. S2.

A multilayer model consisting of finite interfacial regions with enhanced or suppressed thermomechanical properties and an interior bulk-like region is often used to estimate the

overall film T_g as a function of thickness.[28] We estimate the overall film T_g at thicknesses above and below the critical thickness by taking the average value of the superposition model [e.g. Eqs. (4) and (6)]. We compare the results of this model with the simulation results for various film thicknesses ranging from 10 to 60 nm and find good agreement for PS freestanding and PMMA supported films shown as the open and filled symbols, respectively in Fig. 2(c). This provides additional verification that the superposition principle captures the behavior of interacting interphases. We note again, that the parameters describing the local T_g profile are developed at large thicknesses where interphases do not interact. Yet, the local T_g profile over the entire freestanding or supported films can be accurately modeled using superposition of analytical functions with these universal parameters even at significantly low film thicknesses.

Bilayer thin film systems

Now that we have analyzed the T_g behavior of the freestanding and supported films and described how the interactions of interphase regions are approximately additive, we next investigate whether this principle can also be applied to PS–PMMA bilayer thin films. It is known that PS and PMMA polymer melts are immiscible and lead to phase separation in the blend state.[29] In our CG models, we determine the nonbonded monomeric interactions between PS and PMMA by tuning the parameters to match the experimental interfacial tension of a blended system at 425 K, which is approximately 1.5 dyn/cm (see Fig. S1).[29] The methodology to estimate the interfacial tension in the model and calculate the interfacial (i.e., cross interaction) parameters can be found in the Supporting Information. (Interfacial parameters can be found in Table SV.)

After determining the interfacial parameters based on the experimental measurement of the interfacial tension, we systematically investigate the local T_g profile across the PS–PMMA interface. The bilayer film system consists of a 36 nm thick PS layer on top of a 36 nm PMMA layer with periodic boundary conditions in all directions. Due to the disparity between the bulk T_g of the PS and PMMA CG models, we observe a smooth transition of the local T_g from the PMMA phase to the PS phase (Fig. 3). The local composition profile, shown as dotted line in Fig. 3, demonstrates only an approximately ~5 nm thick interface by definition of the Gibbs dividing surface thickness, which agrees with experimental results that report an interfacial layer between 2 and 5 nm for PS–PMMA.[30,31] However, the T_g confinement effect is nearly symmetric and penetrates about 10 nm into both the PS and PMMA phases. This symmetry differs from the results of Baglay and Roth,[14,15] who found that the T_g alteration persists further into the glassy side. However, our results concur with studies performed by Slimani et al. which simulated lamellar diblock copolymer containing a hard and soft phase and reported that the gradient in mobility is found to persist approximately the same length scale in both phases.[32] Discrepancies in the observed interphase length scale and

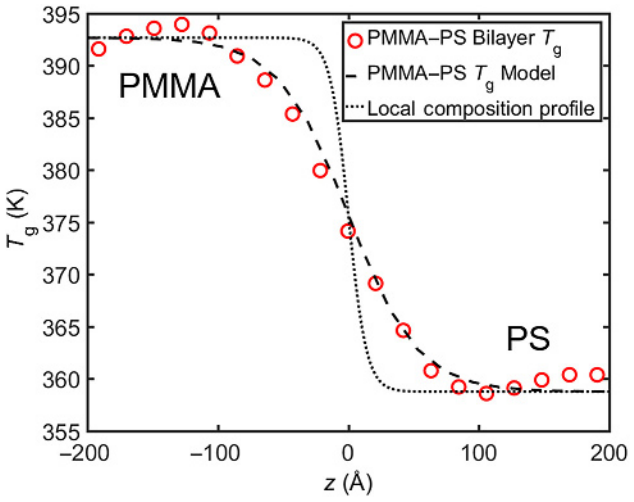

Figure 3. Local T_g profile of PMMA–PS bilayer film interface and local composition profile.

symmetry may be due to the difference in experimental measurement methods as well as sample preparation conditions. The observed length scales of the interphase in the bilayer systems into each layer are also similar to that of the free surface and substrate interphase. We fit the local T_g bilayer interface transition to a function of the form:[14]

$$T_g^{\mathrm{PS-PMMA}}(z) = -A^{\mathrm{bi}}_{\mathrm{PS-PMMA}} \tanh\left(\frac{-z+\mu}{\lambda_{\mathrm{PS-PMMA}}}\right) + \frac{T^{\mathrm{PS}}_{\mathrm{g,bulk}} + T^{\mathrm{PMMA}}_{\mathrm{g,bulk}}}{2}, \quad (5)$$

where $A^{\mathrm{bi}}_{\mathrm{PS-PMMA}} = \left(T^{\mathrm{bulk}}_{\mathrm{g,PMMA}} - T^{\mathrm{bulk}}_{\mathrm{g,PS}}\right)/2$ and $\lambda_{\mathrm{PS-PMMA}}$ is related to the size of the interphase region. Here, μ correlates with the midpoint of the transition region, which reduces to zero when choosing the x-y plane to bisect the PS–PMMA interface.

These results are combined with the analysis of supported and freestanding films to predict the behavior of supported PS–PMMA bilayer films. A 2 to 36 nm PMMA lower-layer is deposited on an attractive substrate, which interacts with the film with interfacial energy consistent with previous conditions. We place a PS upper-layer on top of the PMMA lower-layer, which we maintain at 18 nm thickness. The resulting local T_g profile for the bilayer film demonstrates a maximum of five distinct regimes [Fig. 4(a)]. This reflects T_g-nanoconfinement occurring as a result of the three interfaces, PS–air, PS–PMMA, and PMMA–substrate, as well as bulk-like convergence regions for the PS and PMMA layers between the interphases. When each layer thickness is greater than the respective critical thickness (i.e., $H^{\mathrm{bi}}_{\mathrm{crit,PS}} = \xi^{\mathrm{fs}}_{\mathrm{PS}} + \xi^{\mathrm{bi}}_{\mathrm{PS-PMMA}} \approx 22$ nm, $H^{\mathrm{bi}}_{\mathrm{crit,PMMA}} = \xi^{\mathrm{sp}}_{\mathrm{PMMA}} + \xi^{\mathrm{bi}}_{\mathrm{PS-PMMA}} \approx 18$ nm), we are able to observe all five different regimes within the bilayer film system.

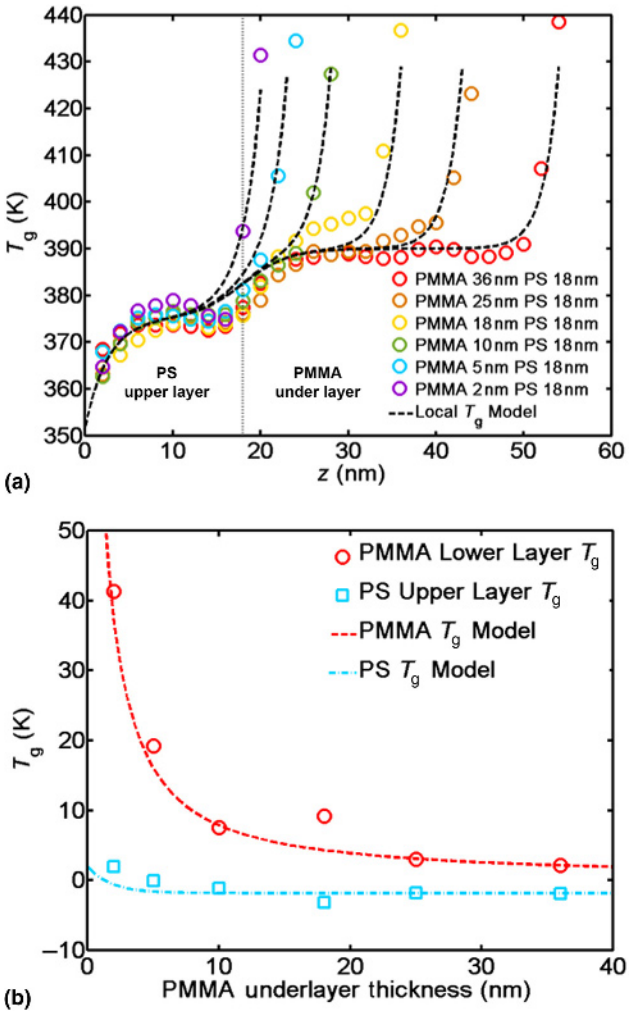

Figure 4. (a) Local T_g results for supported PMMA–PS bilayer film. (b) Resulting layer T_g calculated from simulation compared with the averaged local superposed T_g model.

Locating the *z*-axis at the PS–air interface and pointing into the film, (1) The first regime at the PS–air interface shows a T_g depression indicating higher mobility at the surface which converges to the PS bulk T_g after ~12 nm. (2) The second regime consists of a plateau region representing the bulk-like interior of the PS layer. In our study, the 18 nm PS film is below the critical thickness, and, hence, only a pseudo-convergence region with T_g about 5 to 10 K above the bulk PS T_g can be detected. (3) The third regime is indicative of the ~25 K T_g transition at the PS-PMMA polymer–polymer interface. (4) The fourth regime consists of a plateau region for the PMMA bulk-like interior region, which emerges above the critical thickness. (5) Finally, we see a fifth regime where the PMMA interior region T_g transitions to enhanced T_g at the PMMA–substrate interface which can locally attain values that are 30–40 K above the PMMA bulk T_g near the substrate. Larger PMMA layer thicknesses above $H^{bi}_{crit,PMMA}$ display each of the regions 3–5 in the lower-layer. However, as the PMMA layer thickness decreases below $H^{bi}_{crit,PMMA}$, regime 3–5 begin to overlap and a clear distinction between the PMMA-substrate and PS–PMMA interphases does not exist. We confirm that the interactions between the three dissimilar interphase regions in bilayer films are also additive. We derive the master profile for the local T_g of the supported bilayer film using superposition (Eq. S2), which we apply to the PS-PMMA bilayer system for different PMMA thicknesses from 2 to 36 nm. We find that the model matches the simulation results remarkably well for all lower-layer thicknesses as shown in Fig. 4(a). (Fitting equations for bilayer films can be found in the Supporting Information, and parameters are included in Table SIV.)

The overall T_g for each individual layer is estimated by averaging the superposed local T_g function (Eq. S2) over each polymer phase. These model results are compared with the overall T_g for both the PMMA lower-layer and PS upper-layer from simulation, illustrating strong agreement between the model and simulations [Fig. 4(b)]. For PMMA lower-layer thicknesses much greater than $H^{bi}_{crit,PMMA}$, the PMMA T_g converges to within 0.5% of the bulk value at around 40 nm. As the PMMA lower-layer reduces in thickness, the PMMA–substrate interphase regime becomes an increasing portion of the PMMA layer by volume, which results in an appreciated T_g up to 40 K greater than the bulk when the PMMA layer thickness reaches 2 nm. Interestingly, any free surface effect for the PS layer is eliminated at almost all lower-layer thicknesses. This is consistent with the findings from Roth et al., who showed a suppressed free surface effect on the upper PS layer in bilayer films with a supported PMMA or P2VP lower-layer.[10,11] Roth et al. attributed this finding to slower cooperative segmental motion near the attractive substrate, which persists through the lower-layer film thickness and across the polymer–polymer interface even for films up to 500 nm in thickness. Alternatively, they suggest the higher T_g of PMMA (393 K Bulk T_g) or P2VP (374 K Bulk T_g) relative to the PS layer may also cause the free surface effect to be suppressed.

Looking at the local T_g bilayer data in Fig. 4(a), we find that this occurs due to increased T_g in the PS phase near the PS–PMMA interface arising from the disparity in T_g between PS and PMMA. Specifically, because PMMA has a ~25 K higher bulk T_g than PS in the CG model, this so-called "soft" polymer–polymer interfacial nanoconfinement causes a smooth transition region in the PS phase where the local T_g is enhanced and persists ~10 nm into the PS layer. This effectively cancels the ~28 K T_g reduction found in the PS free surface interphase, which has a similar length scale of ~12 nm before converging to the interior region T_g. This result suggests that substrate effects in the PMMA lower-layer are not the direct cause of elimination of T_g reduction in the PS upper-layer, since the substrate interphase does not overlap with the PS layer for films above the critical thickness. However, we do find that PMMA-substrate effects can alter the PS upper-layer when the PMMA layer is sufficiently thin. At lower-layer thicknesses

that are less than 5 nm, the PMMA-substrate interphase is able to penetrate the PS–PMMA interface and further augment the T_g of the PS layer. Although the appreciation in PS layer T_g is small, it is clear that this occurs from the enhanced local T_g at the PS–PMMA interface at $z = 18$ nm, which is found to be ~394 K for the 2 nm PMMA layer condition in Fig. 4(a). This evidence supports the potential mechanism suggested by Roth et al., that arrested segmental motion near the attractive substrate can persist through the supporting layer and penetrate through the soft polymer interface.[10] However, we find that this only occurs at very thin film layer thicknesses. Because the interphase length scales we measure are of the order of ~10 nm, as compared with several tens of nm through fluorescence methods, we find that penetration of the substrate effect through the PS–PMMA interface only applies for extremely thin lower-layers below 5 nm.

Conclusions

Studies on monolayer and bilayer systems over the past decade have shown that interphase regions on the length scale of tens of nanometers can have a large effect when the characteristic feature size approaches nanoscale dimensions. This understanding has helped explain how the overall thermomechanical properties deviate from the bulk for sufficiently thin homopolymer films. However, more recent studies on multilayer films, blends, block copolymer systems, and nanocomposites, have demonstrated thermomechanical behavior that has not yet been definitively interpreted. TCCG models uniquely enable us to measure local T_g gradients at nanometer resolution for each of the interface types occurring in PS–PMMA bilayer systems.

In particular, we characterize the local T_g profile at free surfaces and supported interfaces and demonstrate that the gradient size and shape are independent of the thickness above the critical thickness H_{crit}, where the various interphases converge to the interior bulk-like T_g and do not overlap with one another. Below the critical thickness H_{crit} where interphase regions are unable to converge to the interior bulk-like T_g and overlap with one another, the combined effect of both similar and dissimilar interphases are approximately additive, and can be estimated by the superposition of local T_g gradient functions without changing fitting parameters. This significant result suggests a framework to predict the spatial T_g in complex microphase-separated systems as a function of geometry at a wide range of characteristic length scales of local polymer phases.

We also measure the local T_g at the PS–PMMA interface and show that the interphase length scale is much larger than the compositional interface itself, and penetrates approximately the same distance (~10 nm) into both phases. Moreover, the length scale of soft polymer interphase propagation into each layer is similar to that of the free surface and substrate interphase. Using this information, we show that the local T_g of the entire supported PS–PMMA bilayer film can be predicted as a function of lower-layer thickness by superposing the gradient functions for each interphase type. The overall layer T_g in all configurations is also accurately captured by the average of the local T_g functions.

Through understanding the local behavior, we are able to provide insight into recent experimental PS–PMMA bilayer results. We find that T_g enhancement in the PS phase at the PS–PMMA interface cancels out the PS-air free surface effect when PMMA is used as the lower-layer. This effect is found to be largely independent of the PMMA lower-layer thickness. We also see that arresting of segmental motion at the attractive substrate-PMMA interphase does not have a long-range effect on the PS layer T_g except at exceedingly thin lower-layer thicknesses where penetration of the substrate effect can occur across the soft polymer interface. This provides evidence of two different mechanisms in which polymer layers can affect the overall T_g of neighboring phases. Our findings provide an explanation of previously observed experimental phenomena in bilayer films, help elucidate the resulting local behavior of overlapping interphase regions, and provide a potential framework to predict the local and overall T_g behavior of multilayer films, copolymers, and nanocomposites.

Supplementary Material Available: Additional supporting information has been provided regarding: (1) interfacial tension calculation methodology, (2) local T_g results for supported PS film, (3) predictive models for local Bilayer T_g behavior, and (4) tables containing local T_g function parameters and CG potential parameters.

Supplementary material

The supplementary material for this article can be found at https://doi.org/10.1557/mrc.2017.113

Acknowledgment

The authors acknowledge support by the Dow Chemical Company and from the Department of Civil & Environmental Engineering, Mechanical Engineering and Materials Science and Engineering at Northwestern University. The authors acknowledge support by the National Institute of Standards and Technology (NIST) through the Center for Hierarchical Materials Design (CHiMaD). W.X. gratefully acknowledges the support from the NIST-CHiMaD Postdoctoral Fellowship. A supercomputing grant from Quest HPC System at Northwestern University is acknowledged.

References

1. M. Ediger and J. Forrest: Dynamics near free surfaces and the glass transition in thin polymer films: a view to the future. *Macromol.* **47**, 471 (2013).
2. C.J. Ellison and J.M. Torkelson: The distribution of glass-transition temperatures in nanoscopically confined glass formers. *Nat. Mater.* **2**, 695 (2003).
3. J. Forrest, K. Dalnoki-Veress, J. Stevens, and J. Dutcher: Effect of free surfaces on the glass transition temperature of thin polymer films. *Phys. Rev. Lett.* **77**, 2002 (1996).
4. P.Z. Hanakata, J.F. Douglas, and F.W. Starr: Interfacial mobility scale determines the scale of collective motion and relaxation rate in polymer films. *Nat. Commun.* **5**, 4163 (2014).

5. D.D. Hsu, W. Xia, J. Song, and S. Keten: Glass-transition and side-chain dynamics in thin films: explaining dissimilar free surface effects for polystyrene vs poly (methyl methacrylate). *ACS Macro Lett.* **5**, 481 (2016).
6. K. Paeng and M. Ediger: Molecular motion in free-standing thin films of poly (methyl methacrylate), poly (4-tert-butylstyrene), poly (α-methylstyrene), and poly (2-vinylpyridine). *Macromol.* **44**, 7034 (2011).
7. K. Paeng, R. Richert, and M. Ediger: Molecular mobility in supported thin films of polystyrene, poly (methyl methacrylate), and poly (2-vinyl pyridine) probed by dye reorientation. *Soft Mat.* **8**, 819 (2012).
8. W. Xia, S. Mishra, and S. Keten: Substrate vs. free surface: competing effects on the glass transition of polymer thin films. *Polymer* **54**, 5942 (2013).
9. C. Ye, C.G. Wiener, M. Tyagi, D. Uhrig, S.V. Orski, C.L. Soles, B.D. Vogt, and D.S. Simmons: Understanding the decreased segmental dynamics of supported thin polymer films reported by incoherent neutron scattering. *Macromol.* **48**, 801 (2015).
10. C.B. Roth, K.L. McNerny, W.F. Jager, and J.M. Torkelson: Eliminating the enhanced mobility at the free surface of polystyrene: fluorescence studies of the glass transition temperature in thin bilayer films of immiscible polymers. *Macromol.* **40**, 2568 (2007).
11. H. Yoon, and G.B. McKenna: Substrate effects on glass transition and free surface viscoelasticity of ultrathin polystyrene films. *Macromol.* **47**, 8808 (2014).
12. N.B. Tito, J.E. Lipson, and S.T. Milner: Lattice model of mobility at interfaces: free surfaces, substrates, and bilayers. *Soft Mat.* **9**, 9403 (2013).
13. C.B. Roth, and J.M. Torkelson: Selectively probing the glass transition temperature in multilayer polymer films: equivalence of block copolymers and multilayer films of different homopolymers. *Macromol.* **40**, 3328 (2007).
14. R.R. Baglay, and C.B. Roth: Communication: experimentally determined profile of local glass transition temperature across a glassy-rubbery polymer interface with a T_g difference of 80 K. *J. Chem. Phys.* **143**, 111101 (2015).
15. R.R. Baglay, and C.B. Roth: Local glass transition temperature $T_g(z)$ of polystyrene next to different polymers: hard vs. soft confinement. *J. Chem. Phys.* **146**, 203307 (2017).
16. R.J. Lang, W.L. Merling, and D.S. Simmons: Combined dependence of nanoconfined T_g on interfacial energy and softness of confinement. *ACS Macro Lett.* **3**, 758 (2014).
17. R.P. White, C.C. Price, and J.E. Lipson: Effect of interfaces on the glass transition of supported and freestanding polymer thin films. *Macromol.* **48**, 4132 (2015).
18. D.D. Hsu, W. Xia, S.G. Arturo, and S. Keten: Systematic method for thermomechanically consistent coarse-graining: a universal model for methacrylate-based polymers. *J. Chem. Theory Comput.* **10**, 2514 (2014).
19. D.D. Hsu, W. Xia, S.G. Arturo, and S. Keten: Thermomechanically consistent and temperature transferable coarse-graining of atactic polystyrene. *Macromol.* **48**, 3057 (2015).
20. M.C. Payne, M.P. Teter, D.C. Allan, T. Arias, and J. Joannopoulos: Iterative minimization techniques for ab initio total-energy calculations: molecular dynamics and conjugate gradients. *Rev. Mod. Phys.* **64**, 1045 (1992).
21. W.G. Hoover: Canonical dynamics: equilibrium phase-space distributions. *Phys. Rev. A* **31**, 1695 (1985).
22. S. Plimpton and B. Hendrickson: A new parallel method for molecular dynamics simulation of macromolecular systems. *J. Comput. Chem.* **17**, 326 (1996).
23. M. Marvin, R. Lang, and D. Simmons: Nanoconfinement effects on the fragility of glass formation of a model freestanding polymer film. *Soft Mat.* **10**, 3166 (2014).
24. Y. Zhou and S.T. Milner: Short-time dynamics reveals T_g suppression in simulated polystyrene thin films. *Macromol.* **50**, 5599 (2017).
25. J. DeFelice, S.T. Milner, and J.E.G. Lipson: Simulating local T_g reporting layers in glassy thin films. *Macromol.* **49**, 1822 (2016).
26. A.N. Rissanou and V. Harmandaris: Structural and dynamical properties of polystyrene thin films supported by multiple graphene layers. *Macromol.* **48**, 2761 (2015).
27. W. Xia, J. Song, D.D. Hsu, and S. Keten: Side-group size effects on interfaces and glass formation in supported polymer thin films. *J. Chem. Phys.* **146**, 203311 (2017).
28. J.A. Forrest and J. Mattsson: Reductions of the glass transition temperature in thin polymer films: probing the length scale of cooperative dynamics. *Phys. Rev. E* **61**, R53 (2000).
29. P. Ellingson, D. Strand, A. Cohen, R. Sammler, and C. Carriere: Molecular weight dependence of polystyrene/poly (methyl methacrylate) interfacial tension probed by imbedded-fiber retraction. *Macromol.* **27**, 1643 (1994).
30. S.H. Anastasiadis, T.P. Russell, S.K. Satija, and C.F. Majkrzak: The morphology of symmetric diblock copolymers as revealed by neutron reflectivity. *J. Chem. Phys.* **92**, 5677 (1990).
31. M. Fernandez, J. Higgins, J. Penfold, R. Ward, C. Shackleton, and D. Walsh: Neutron reflection investigation of the interface between an immiscible polymer pair. *Polymer* **29**, 1923 (1988).
32. M.Z. Slimani, A.J. Moreno, and J. Colmenero: Heterogeneity of the segmental dynamics in lamellar phases of diblock copolymers. *Macromol.* **44**, 6952 (2011).